Langmuir
Article
pubs.acs.org/Langmuir

Nanochemistry in Confined Environments: Polyelectrolyte Brush-Assisted Synthesis of Gold Nanoparticles inside Ordered Mesoporous Thin Films

Alejandra Calvo,[†] M. Cecilia Fuertes,[†] Basit Yameen,[‡] Federico J. Williams,[§,∥] Omar Azzaroni,*[,⊥] and Galo J. A. A. Soler-Illia*[,†,∥]

[†]*Gerencia de Química, Comisión Nacional de Energía Atómica (CNEA), Argentina,* [‡]*Max-Planck-Institut für Polymerforschung, Mainz, Germany,* [§]*INQUIMAE, Facultad de Ciencias Exactas y Naturales Universidad de Buenos Aires, Argentina,* [∥]*Depto de Química Inorgánica, Analítica y Química Física, Facultad de Ciencias Exactas y Naturales Universidad de Buenos Aires, Argentina, and* [⊥]*Instituto de Investigaciones Fisicoquímicas Teóricas y Aplicadas (INIFTA), Depto. de Química, Facultad de Ciencias Exactas, Universidad Nacional de La Plata, CONICET, Argentina*

Received October 9, 2009. Revised Manuscript Received December 29, 2009

A robust and straightforward strategy allowing the controlled confinement of metal nanoparticles within the 3D framework of mesoporous films is presented. The chemical methodology is based on the inner surface modification of mesoporous silica films with polyelectrolyte brushes. We demonstrate that the macromolecular building blocks significantly enhance the site-selective preconcentration of nanoparticle precursors in the inner environment of the mesoporous film. Then, chemical reduction of the preconcentrated precursors led to the formation of metal nanoparticles locally addressed in the mesoporous structure. We show that the synergy taking place between two versatile functional nanobuilding blocks (ordered mesocavities and polymer brushes) can produce stable embedded nanoparticles with tuned optical properties in a very simple manner. As a general framework, the strategy can be easily adapted to different sets of polymer brushes and mesoporous films in order to regulate the monomer−precursor interactions and, consequently, manipulate the site-selective character of the different chemistries taking place in the film. We consider that the "integrative chemistry" approach described in this work provides new pathways to manipulate the physicochemical characteristics of hybrid organic−inorganic advanced functional assemblies based on the rational design of chemistry and topology in confined environments.

Introduction

During the past decades, the creativity of chemists and materials scientists provided a means for developing a wide variety of nanostructured materials with unprecedented functional properties.[1,2] Most of this progress stemmed from interdisciplinary work exploiting chemistry as a key enabler to rationally design molecular building blocks and nanomaterials entirely from scratch.[3] As the knowledge began to accumulate, this led to an emerging concept bridging the gap between molecular materials chemistry and nanotechnology, which is often referred to as "nanochemistry".[4,5] Today we have a mature discipline whose high standards are challenging to meet. Yet, it represents a unique and versatile toolbox to achieve actual molecular design of materials.[6] Nanochemistry has allowed us to access the molecular processes taking place in confined geometries that are formed using various classes of materials, such as inverse micelles, supramolecular architectures, biomolecular nanocapsules, self-organized block copolymers, or solid-state nanopores.[7] The chemical processes that occur in constrained spaces deserve particular attention due to they are a fundamental part of many synthetic procedures commonly used in nanoscience and nanotechnology.[8] In a physically constrained environment, interfacial interactions, symmetry breaking, and confinement-induced entropy loss can play dominant roles in determining molecular organization or chemical reactivity.[9] In some cases it has been suggested that nanoscale confinement could be harnessed as a "synthetic tool" to modify materials' properties.[10]

Of particular interest are the processes that take place inside mesoporous materials ($2\ \text{nm} < d_{\text{pore}} < 50\ \text{nm}$). Confinement inside a mesopore can significantly change the interaction between molecules and their surroundings.[8,9] In confined spaces of nearly molecular dimensions, all the adsorbed molecules are in close

*Corresponding authors. E-mail: azzaroni@inifta.unlp.edu.ar (O.A.); gsoler@cnea.gov.ar (G.J.A.A.S.-I.).

(1) *Functional Nanomaterials*; Geckeler, K. E., Rosenberg, E., Eds.; American Scientific Publishers: Stevenson Ranch, CA, 2006.

(2) Vollath, D. *Nanomaterials: An Introduction to Synthesis, Properties and Applications* VCH-Wiley: Wienheim, 2008.

(3) Ozin, G. A. *Adv. Mater.* **1992**, *4*, 612.

(4) (a) Ozin, G. A.; Arsenault, A. C.; Cademartiri, L. *Nanochemistry: A Chemical Approach to Nanomaterials*; Royal Society of Chemistry: London, 2009. (b) Ozin, G. A.; Cademartiri, L. *Small* **2009**, *5*, 1240.

(5) *Nanomaterials and Nanochemistry*; Bréchignac, C., Houdy, P., Lahmani, M., Eds.; Springer-Verlag: Heidelberg, 2007.

(6) Descalzo, A. B.; Martínez-Máñez, R.; Sancenón, F.; Hoffmann, K.; Rurack, K. *Angew. Chem., Int. Ed.* **2006**, *45*, 5924.

(7) (a) Turco Liveri, V. In *Controlled Synthesis of Nanoparticles in Microheterogeneous Systems*; Springer-Verlag: Heidelberg, 2006; Chapter 2, pp 75−90. (b) Diana, F. S.; Lee, S.-H.; Petroff, P. M.; Kramer, E. J. *Nano Lett.* **2003**, *3*, 891. (c) Niu, Y. H.; Yeung, L. K.; Crooks, R. M. *J. Am. Chem. Soc.* **2001**, *123*, 6840. (d) Douglas, T.; Dickson, D. P. E.; Betteridge, S.; Charnock, J.; Garner, C. D.; Mann, S. *Science* **1995**, *269*, 54. (e) Lopes, W. A.; Jaeger, H. M. *Nature* **2001**, *414*, 735–738. (f) Yameen, B.; Ali, M.; Neumann, R.; Ensinger, W.; Knoll, W.; Azzaroni, O. *J. Am. Chem. Soc.* **2009**, *131*, 2070. (g) Yameen, B.; Ali, M.; Neumann, R.; Ensinger, W.; Knoll, W.; Azzaroni, O. *Nano Lett.* **2009**, *9*, 2788.

(8) (a) Chernysheva, M. V.; Sapoletova, N. A.; Eliseev, A. A.; Lukashin, A. V.; Tretyakov, Y. D.; Goernert, P. *Pure Appl. Chem.* **2006**, *78*, 1749. (b) Liu, J.; Wei, A. *Chem. Commun.* **2009**, 4254. (c) Tang, X.-P.; Mogilevsky, G.; Kulkarni, H.; Wu, Y. *J. Phys. Chem. C* **2007**, *111*, 18615. (d) Okada, T.; Harada, M.; Ohki, T. *Anal. Sci.* **2009**, *25*, 167. (e) Corriu, R. J. P.; Mehdi, A.; Reyé, C. *J. Mater. Chem.* **2005**, *15*, 4285. (f) Zhao, X.-G.; Shi, J.-L.; Hu, B.; Zhang, L.-X.; Hua, Z.-L. *J. Mater. Chem.* **2003**, *13*, 399.

(9) (a) Goettmann, F.; Sanchez, C. *J. Mater. Chem.* **2007**, *17*, 24. (b) Schoonheydt, R. A.; Weckhuysen, B. M. *Phys. Chem. Chem. Phys.* **2009**, *11*, 2794. (c) Wu, Y.; Cheng, G.; Katsov, K.; Sides, S. W.; Wang, J.; Tang, J.; Frederickson, G. H.; Moskovits, M.; Stucky, G. D. *Nat. Mater.* **2004**, *3*, 816.

(10) Huck, W. T. S. *Chem. Commun.* **2005**, 4143.

interaction with the surface, leading to remarkable consequences in their physical and chemical properties.[11] Materials confined in nanoscale geometries show structures and dynamics different from those exhibited in bulk.[12] The richness of chemical phenomena in confined environments opens the path to advanced applications that rely on designed substrate−surface interactions. In particular, mesoporous oxide thin films (MOTF) provide a sound platform for the creation of ordered arrays of monodisperse cavities that can be nowadays precisely designed and produced in reproducible fashion.[13] Indeed, the synthesis of MOTF by combination of soft chemistry, self-assembly of supramolecular templates, and surface modification permits to create, in very few synthesis steps, well-defined "nanofacilities", where chemical functions can be precisely located in space, in a transparent matrix with tailored diffusion features.

In this context, the combination of MOTF as robust scaffolds[14] and macromolecular architectures[15] as functional building blocks has led to the development of new hybrid advanced materials.[16] The precise incorporation of active elements in robust nanosized 3D networks with tunable surfaces is the cornerstone of the rational design of "on-demand" organic−inorganic hybrid assemblies for multiple applications. The controlled assembly of functional building blocks into the preorganized pore arrays of MOTF is the key step to achieve the fine-tuning of nanostructured architectures, which can be controlled from the local environment to the mesoscopic and macroscopic length scales.[17] Tailoring the inner environment of the inorganic scaffold would require an accurate control over the chemistry but also over the topology of the nanometer-sized 3D networks. This control of the "nanofacilities" opens the gate to performing chemistry in an 8 nm test tube.

The molecular design of hybrid mesoporous assemblies demands a precise control over the density and spatial arrangement of the functional groups incorporated in the pores, i.e., nanochemistry. Within this framework, the synthesis of macromolecular architectures into nanoporous media is emerging as an exciting area of research with strong implications for materials design. The derivatization of nanopore walls of mesoporous materials with well-defined polymers represents a unique tool for designing inorganic−organic hybrid mesoporous assemblies.[18] Considering the chemical diversity of polymers, the macromolecular building blocks can endow the mesoporous scaffold with built-in responses to a myriad of environmental chemical and physical stimuli, thus rendering them with, for example, catalytic, pH-responsive, or permselective properties.[19]

It has been recently proven that the derivatization of mesoporous silica films by surface-initiated polymerization of polyelectrolyte brushes provides a unique strategy for the incorporation of complex chemical functions to the pore system. Grafted polymer brushes dramatically change the transport of ionic probes across modified MOTF. The synergy of controlled cavities and tailored polymeric building blocks provides a novel platform for the controlled design of ion gates.[20] In this work, we demonstrate that the robust anchoring of polycationic macromolecular building blocks in the nanopore walls leads to the creation of an active surface, capable to preconcentrate metallic precursors by anion exchange. Subsequently, a straightforward chemical route leads to the controlled preparation of gold nanoparticles within the derivatized mesoporous films.[21] We show that the controlled formation of polyelectrolyte brushes is indeed a key feature to perform "nanochemistry" in the nanopore environment. This tailored pore modification provides the chemical environment to preconcentrate the gold chlorocomplexes that controls nucleation and growth of gold colloids uniformly dispersed inside the film. This example of a designed synthesis of nanomaterials inside mesoporous films through molecular tuning of the pore features has strong immediate implications for the rational design of inorganic−organic nanocomposites with tailored optical or catalytic properties. We are confident that these results will constitute a key element in the "nanochemistry" toolbox and will trigger new and refreshing ideas to create complex hybrid nanomaterials using rational synthetic tools.

Experimental Section

Synthesis of Mesoporous Amino-Silica Thin Films. Propylamino-functionalized mesoporous thin films were synthesized, as we described in previous works,[20] via the co-condensation of the oxide precursor tetraethoxysilane (TEOS, Merck) and the amine precursor 3-aminopropyltriethoxysilane (APTES, Fluka 98%) in the presence of the template (F127 block copolymer, Aldrich, M = 13 600). The precursor solution was prepared using 0.8 TEOS:0.2 APTES:0.005 F127:24 EtOH:5.2 H_2O:0.28 HCl. This solution was used to produce films by dip-coating on silicon, glass, and ITO substrates under 40−50% relative humidity conditions at 25 °C (1−2 mm s^{-1} withdrawing speed). The organic

(11) (a) Aprile, C.; Abad, A.; García, H.; Corma, A. *J. Mater. Chem.* **2005**, *15*, 4408. (b) Gu, J. L.; Shi, J. L.; You, G. J.; Xiong, L. M.; Qiang, S. X.; Hua, Z. L.; Chen, H. R. *Adv. Mater.* **2005**, *17*, 557. (c) Stein, A.; Melde, B. J.; Schroden, R. C. *Adv. Mater.* **2000**, *12*, 1403. (d) Cortial, G.; Siutkowski, M.; Goettmann, F.; Moores, A.; Boissiére, C.; Grosso, D.; Le Floch, P.; Sanchez, C. *Small* **2006**, *2*, 1042. (e) Henao, J. D.; Suh, Y.-W.; Lee, J.-K.; Kung, M. C.; Kung, H. H. *J. Am. Chem. Soc.* **2008**, *130*, 16142.

(12) (a) Chau, J. L. H.; Leung, A. Y. L.; Shing, M. B.; Yeung, K. L.; Chan, C. M. *Nano Science and Technology: Novel Structures and Phenomena*; Tang, Z., Sheng, P., Eds.; Taylor & Francis: London, 2003; Chapter 27, pp 228−234. (b) Beckstein, O.; Biggin, P. C.; Sansom, M. S. P. *J. Phys. Chem. B* **2001**, *105*, 12902.

(13) Sanchez, C.; Boissière, C.; Grosso, D.; Laberty, C.; Nicole, L. *Chem. Mater.* **2008**, *20*, 682.

(14) (a) See, for example, the special issue dedicated to templated materials: *Chem. Mater.* **2008**, *20* (3). See also: (b) Soler-Illia, G. J. A. A.; Sanchez, C.; Lebeau, B.; Patarin, J. *Chem. Rev.* **2002**, *102*, 4093. (c) Soler-Illia, G. J. A. A.; Innocenzi, P. *Chem.—Eur. J.* **2006**, *12*, 4478. (d) Soler-Illia, G. J. A. A.; Crepaldi, E. L.; Grosso, D.; Sanchez, C. *Curr. Opin. Colloid Interface Sci.* **2003**, *8*, 109.

(15) (a) *Supramolecular Polymers*; Ciferri, A., Ed.; CRC Press: Boca Raton, FL, 2005. (b) Hamley, I. W. In *Introduction to Soft Matter: Synthetic and Biological Self-Assembling Materials*; John Wiley & Sons: West Sussex, 2007.

(16) (a) Gómez-Romero, P.; Sanchez, C. In *Functional Hybrid Materials*; VCH-Wiley: Weinheim, 2004; Chapter 1, pp 1−14. (b) *Hybrid Materials: Synthesis, Characterization and Applications*; Kickelbick, G., Ed.; Wiley-VCH: Weinheim, 2007.

(17) (a) Yoo, S.; Lunn, J. D.; González, S.; Ristich, J. A.; Simanek, E. E.; Shantz, D. F. *Chem. Mater.* **2006**, *18*, 2935. (b) Reynhardt, J. P. K.; Yang, Y.; Sayari, A.; Alper, H. *Adv. Funct. Mater.* **2006**, *15*, 1641. (c) Tian, B.-S.; Yang, C. *J. Phys. Chem. C* **2009**, *113*, 4925. (d) Rzayev, J.; Hillmyer, M. A. *J. Am. Chem. Soc.* **2005**, *127*, 13373. (e) Rosenholm, J. M.; Duchanoy, A.; Lindén, M. *Chem. Mater.* **2008**, *20*, 1126. (f) Rosenholm, J. M.; Penninkangas, A.; Lindén, M. *Chem. Commun.* **2006**, 3909.

(18) (a) Save, M.; Granvorka, G.; Bernard, J.; Charleux, B.; Boissiére, C.; Grosso, D.; Sanchez, C. *Macromol. Rapid Commun.* **2006**, *27*, 393. (b) Ford, D. M.; Simanek, E. E.; Shantz, D. F. *Nanotechnology* **2000**, *16*, S458. (c) Choi, M.; Kleitz, F.; Liu, D.; Lee, H. Y.; Ahn, W.-S.; Ryoo, R. *J. Am. Chem. Soc.* **2005**, *127*, 1924. (d) Kruk, M.; Dufour, B.; Celer, E. B.; Kowalewski, T.; Jaroniec, M.; Matyjaszewski, K. *Macromolecules* **2008**, *41*, 8584. (e) Kruk, M.; Dufour, B.; Celer, E. B.; Kowalewski, T.; Jaroniec, M.; Matyjaszewski, K. *J. Phys. Chem. B* **2005**, *109*, 9216. (f) Moreno, J.; Sherrington, D. C. *Chem. Mater.* **2008**, *20*, 4468.

(19) (a) *Responsive Polymer Materials: Design and Applications*; Minko, S., Ed.; Blackwell Publishing: Ames, 2006. (b) Azzaroni, O.; Trappmann, B.; van Rijn, P.; Zhou, F.; Kong, B.; Huck, W. T. S. *Angew. Chem., Int. Ed.* **2006**, *45*, 7440. (c) Yameen, B.; Kaltbeitzel, A.; Langner, A.; Duran, H.; Müller, F.; Gösele, U.; Azzaroni, O.; Knoll, W. *J. Am. Chem. Soc.* **2008**, *130*, 13140. (d) Azzaroni, O.; Zheng, Z.; Yang, Z.; Huck, W. T. S. *Langmuir* **2006**, *26*, 6730. (e) Barbey, R.; Lavanant, L.; Paripovic, D.; Schüwer, N.; Sugnaux, C.; Tugulu, S.; Klok, H.-A. *Chem. Rev.* **2009**, *109*, 5437. (f) Ayres, N. *Polym. Chem.* **2010**, DOI: 10.1039/b9py00246d.

(20) (a) Calvo, A.; Yameen, B.; Williams, F. J.; Azzaroni, O.; Soler-Illia, G. J. A. A. *Chem. Commun.* **2009**, 2553. (b) Calvo, A.; Yameen, B.; Williams, F. J.; Soler-Illia, G. J. A. A.; Azzaroni, O. *J. Am. Chem. Soc.* **2009**, *131*, 10866. (c) Schepelina, O.; Zharov, I. *Langmuir* **2008**, *24*, 14188.

(21) (a) Fukuoka, A.; Araki, H.; Sakamoto, Y.; Sugimoto, N.; Tsukada, H.; Kumai, Y.; Akimoto, Y.; Ichikawa, M. *Nano Lett.* **2002**, *2*, 793. (b) Mukherjee, P.; Patra, C. R.; Ghosh, A.; Kumar, R.; Sastry, M. *Chem. Mater.* **2002**, *14*, 1678. (c) Petkov, N.; Stock, N.; Bein, T. *J. Phys. Chem. B* **2005**, *109*, 10737. (d) Fan, H.; Yang, K.; Boye, D. M.; Sigmon, T.; Malloy, K. J.; Xu, H.; López, G. P.; Brinker, C. J. *Science* **2004**, *304*, 567.

template was removed by extraction in 0.01 mol dm^{-3} HCl in absolute ethanol (Merck) for 3 days under stirring.

Anchoring 4,4′-Azobis(4-cyanopentanoic acid) on Mesoporous Amino-Silica Films. The surface modification of the mesoporous amino-silica film with azo initiator groups was accomplished following the procedure reported by Bruening and co-workers with only minor modifications.[27] Briefly, 0.5 g (1.78 mmol) of 4,4′-azobis(4-cyanopentanoic acid) and 0.92 g (4.5 mmol) of DCC were added to a single-neck Schlenk flask and closed with a rubber septum. The reactants were degassed under vacuum for 15 min followed by backfilling with N_2(g). 40 mL of dry DMF was added to the flask through the septum with the help of a syringe, and the reactants were allowed to dissolve. After complete dissolution 0.13 mL of dry pyridine was added. Mesoporous samples were sealed in Schlenk tubes and degassed (4 × high-vacuum pump/N_2 refill cycles). Then, the reaction mixture was syringed into the Schlenk flasks containing the azo-modified films and left overnight under N_2(g) at room temperature. Finally, the mesoporous substrates were removed from the reaction mixture and immersed in a beaker containing DMF. The beaker was gently shaken over a period of 2 h. The modified substrates were then washed twice with DMF followed by washing with water and ethanol. The initiator-functionalized mesoporous films were store under nitrogen below 4 °C until further use.

Poly(2-methacryloyloxy)ethyltrimethylammounium Chloride Brush Growth on Initiator-Functionalized Mesoporous Silica Films. In a 100 mL Schlenk flask, 23.3 g of the monomer (2-methacryloyloxy)ethyltrimethylammounium chloride as 75 wt % solution in water was added. The monomer solution was diluted with water to make it 50 wt %. This solution was degassed by N_2(g) bubbling for 1 h. The initiator-functionalized single mesoporous silica substrate was sealed in a Schlenk tube and degassed (4 × high-vacuum pump/N_2 refill cycles). The degassed monomer solution was syringed into this Schlenk flask adding enough to wholly immerse the substrate. The flask was immersed in an oil bath preheated to 65 °C. The polymerization was carried out at 65 °C for 40 min. The mesoporous silica substrate was then removed from the polymerization solution and washed extensively with water. The obtained poly(2-methacryloyloxy)ethyltrimethylammounium chloride brush grafted mesoporous silica was dried under a stream of N_2(g) and stored in tightly closed container until further use.

Au Nanoparticle Synthesis. Au nanoparticles (NPs) were synthesized within mesoporous thin films as follows: films were immersed in an aqueous solution of 1 mM $HAuCl_4$ (pH ∼ 1) for 30 min (preconcentration step). The films were washed several times with deionized water in order to remove non ion-paired precursors. Then they were introduced in 0.5 mM $NaBH_4$ solution for 30 s (chemical reduction step), rinsed with deionized water, and dried with a stream of N_2 at room temperature. This procedure was carried out for PMETAC-modified silica films and amino-silica films.

Characterization. Transmission electron microscopy (TEM) imaging was performed using a Philips EM-301 TEM microscope, operated at 60 keV. TEM samples were prepared by placing scratched films on a carbon-coated copper grid (200 mesh). Film mesostructure was analyzed by SAXS with two-dimensional detection at the D11A-SAXS2 line at the Laboratório Nacional de Luz Síncrotron, Campinas, SP, Brazil (LNLS), using $\lambda = 1.608$ Å, a sample−detector distance of 650 mm, and a CCD detector (3° incidence). Diffuse reflectance infrared Fourier transform spectroscopy measurements (DRIFTS) were performed on a Nicolet Magna 560 instrument, equipped with a liquid nitrogen-cooled MCT-A detector. DRIFTS measurements were performed by depositing scratched film samples on a KBr filled DRIFTS sample holder. X-ray photoelectron spectroscopy (XPS) measurements were obtained using a Specs Sage 150 spectrometer equipped with a dual anode Mg/Al X-ray source and a hemispherical electron energy analyzer. Quoted binding energies (BEs) are referred to the adventitious C 1s emission at 285 eV. Quantitative calculations were carried out from the integrated intensities of N 1s core levels. X-ray reflectometry (XRR) measurements were performed at the D10A-XRD2 line of Laboratório Nacional de Luz Síncrotron, Campinas, SP, Brazil ($\lambda = 1.5498$ Å). In order to obtain accurate density values, measurements were performed under low-humidity conditions (under a stream of dry nitrogen). This is a relevant experimental aspect, as the condensation of atmospheric moisture within the pores could lead to a severe underestimation of the film mesoporosity. Optical characterization by UV−vis spectroscopy was performed employing a Hewlett-Packard 8453 spectrophotometer in transmission mode; films were deposited on glass substrates. Water adsorption curves (at 298 K) were measured by environmental ellipsometric porosimetry (EEP, SOPRA GES5A). Film thickness and refractive index values were obtained from the ellipsometric parameters ψ and Δ under nitrogen flux containing variable water vapor quantities; P/P_{sat} was varied from 0 to 1 (P_{sat} being the saturation water vapor at 298 K). Film pore volume and pore size distribution at each P/P_{sat} were obtained by modeling the refractive index obtained according to a three-medium Bruggeman effective medium approximation (BEMA); pore size distributions were obtained from the analysis of the refractive index variation, using the WinElli 2 software (SOPRA, Inc.).

Results and Discussion

Derivatization of Mesoporous Silica Films with Polyelectrolyte Brushes. Molecular Design of the Pore Environment. Performing "nanochemistry" in confined environments demands a careful control of the pore properties, such as surface energy, charge density, and functional group composition. The synthesis of metal colloids in porous environments has been almost exclusively based on the impregnation of precursor species, i.e., $AuCl_4^-$, onto the mesoporous silica with subsequent reduction of the ionic precursor to generate the metal nanoparticles.[21b] In principle, the functional groups incorporated within the channel pores of the mesostructured film should facilitate the anchoring of the metal precursor exclusively within the internal surface of the mesoporous substrate by strong interactions between the precursors and the surface functional groups. This is a key aspect that helps to preclude the formation of nanoparticles in the external part of the film.

The isoelectric point (IEP) of the support matrix plays a key role in the successful incorporation and dispersion of metal precursors into the nanostructured support. The prerequisite for the successful incorporation of metal precursors requires the strong interaction of the anionic chloro complexes with a positively charged oxide surface.[19] This explains why impregnation processes of anionic precursors in slightly acidic conditions proceed straightforwardly in high IEP mesoporous oxides, like titania (IEP ∼ 6.0).[22] Conversely, the low isoelectric point of silica (IEP ∼ 2) poses a completely different scenario.[23] The mesoporous silica is highly negatively charged under the typical impregnation conditions of $AuCl_4^-$ species, and consequently, no coordination of the Au precursors is expected. Therefore, the direct wet impregnation method could not be used to prepare gold nanoparticles in bare mesoporous SiO_2 unless the proper adjustment of the isoelectric point of the host matrix is done. This should be accomplished in such a way that a major fraction of the population of anionic $AuCl_4^-$ complexes is bound or at least adsorbed onto the mesoporous surface.

(22) Kolsmulski, M. *J. Colloid Interface Sci.* **2002**, *253*, 77.
(23) Calvo, A.; Angelomé, P. C.; Sánchez, V. M.; Scherlis, D. A.; Williams, F. J.; Soler-Illia, G. J. A. A. *Chem. Mater.* **2008**, *20*, 4661.

In this context, coating the silica walls with cationic polyelectrolyte brushes is a potentially useful strategy for incorporating a range of organic functional groups which could open up new methodologies to chemically modify the nanostructured host matrix.

We used amino-functionalized mesoporous silica films ($R-NH_2$:Si 0.2:1) as a platform to build up the hybrid organic−inorganic assemblies. Films were produced by dip-coating on silicon, glass, or indium tin oxide (ITO) substrates using Pluronics F127 block copolymer as the structure directing agent.[23,24] Films exposed to successive consolidation and extraction process displayed highly organized pore arrays with cubic-derived mesostructure ($Im\bar{3}m$); the cubic cell parameter a was calculated to be 19.6 nm from analysis of the off-plane [110] reflection of the SAXS pattern. Films undergo a uniaxial contraction perpendicularly to the substrate (45% thickness reduction) after a consolidation thermal treatment at 200 °C followed by template extraction, leading to pores with an ellipsoidal shape. Pore volume and pore size can be calculated from the water sorption isotherms obtained from ellipsometric porosimetry measurements (see ESI). A pore volume of 26% and an average major pore diameter of ca. 9 nm (calculated from the isotherm adsorption branch) were determined by water sorption ellipsometric porosimetry measurements, according to the model proposed by Boissière et al. for ellipsoidal mesopores;[25] neck sizes (from the desorption branch) are in the order of 3 nm diameter.

The surface density of amino groups in the host matrix is highly reproducible, and their reactivity has been described in detail in a recent publication.[24] Pores are accessible after template removal, and ∼16% of the total population of amine groups is available for reacting on the pore walls. These surface amino groups were used as grafting sites for the surface-initiated polymerization[26] of poly 2-(methacryloyloxy)ethyltrimethylammonium chloride) (PMETAC) brushes. Briefly, the amino groups were initially conjugated to 4,4′-azobis(4-cyanopentanoic acid), which acted as the surface-confined polymerization initiator.[27] Subsequently, brush growth was accomplished by surface-initiated radical polymerization of the METAC monomers in the presence of the adequate solvent during a preset reaction time (see Experimental Section for details). Chemical modification with PMETAC brushes was confirmed and quantified by diffuse infrared Fourier transform spectroscopy (DRIFTS) and X-ray photoelectron spectroscopy (XPS), respectively.

Figure 1a (dotted trace) shows a typical DRIFTS spectrum of an amino-silica film, which displays the bands corresponding to the inorganic matrix: Si−OH and Si−O−Si stretching at ∼966 and ∼1080 cm^{-1}, respectively. The characteristic N−H asymmetric bending bands belonging to amine group are found at ∼1560 cm^{-1}. After polymerization (solid trace), these bands remained the same but two new bands appeared at ∼1140 and ∼1727 cm^{-1}. These signals were attributed to the presence of the C−O−C asymmetric stretching and C=O stretching of ester groups, respectively.[28] This observation is in accordance with the chemical structure of the polyelectrolyte (see Figure 1b) in which each monomer unit is linked to the polymer backbone through an ester linkage. Once the DRIFTS analysis corroborated the presence of the PMETAC brush, we proceeded to a quantitative analysis using XPS to estimate the degree of polymerization of the polymer brush in the mesoporous film. Because of the high porosity of the film, the probing depth of our measurements was estimated to be ∼9 nm.[24] As a consequence, XPS probes the film surface, pore openings, and film walls up to a thickness of two pore layers after the film contraction caused by thermal treatment. Figure 1b shows the N 1s XP spectra of a sample prior to and after modification with PMETAC brushes. The XPS signal describes a significant change after the surface-initiated polymerization reaction. In the amino-silica spectrum there is solely one contribution at ∼400 eV, which corresponds to $-NH_2$ groups. In contrast, the PMETAC spectrum clearly shows two different contributions: the first one, at ∼400 eV, is similar to the one observed in amino-silica and is attributed to the amino groups remaining inside the oxide matrix without reacting; the more intense peak observed at ∼402.5 eV is attributed to the quaternary ammonium groups in the polymer brush.

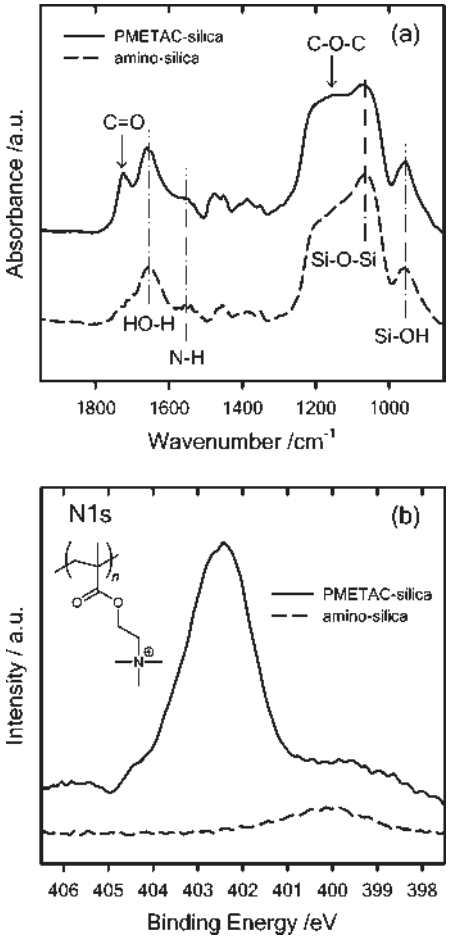

Figure 1. DRIFT (a) and XPS (b) spectra corresponding to the chemical characterization of the amino-silica mesoporous films prior to (dotted trace) and after (solid trace) the surface-initiated polymerization of PMETAC brushes. The chemical structure of the cationic polyelectrolyte is also depicted.

Considering that the analysis involves only one atomic core level (N 1s), quantitative analysis can be performed without requiring signal deconvolution. Instrumental and photoionization cross-section corrections were considered negligible. The difference between the integrated intensity of the total N 1s signal prior to (I_{SA}) and after (I_{PMETAC}) brush growth is proportional to the total number of monomers incorporated during the

(24) Calvo, A.; Joselevich, M.; Soler-Illia, G. J. A. A.; Williams, F. J. *Microporous Mesoporous Mater*. **2009**, *121*, 67.
(25) Boissière, C.; Grosso, D.; Lepoutre, S.; Nicole, L.; Brunet-Bruneau, A.; Sanchez, C. *Langmuir* **2005**, *21*, 12362.
(26) Advincula, R. In *Surface-Initiated Polymerization I*; Jordan, R., Ed.; Springer-Verlag: Heidelberg, 2006; p 107.
(27) Huang, W.; Skanth, G.; Baker, G. L.; Bruening M.L., M. L. *Langmuir* **2001**, *17*, 1731.
(28) Socrates, G. *Infrared and Raman Characteristic Group Frequencies*, 3rd ed.; John Wiley & Sons: Chichester, 2001.

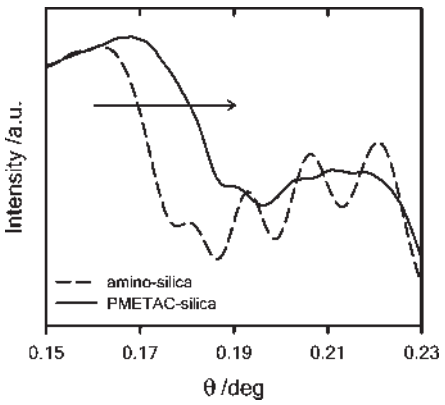

Figure 2. X-ray reflectivity data corresponding to the mesoporous silica films prior to (dotted trace) and after (solid trace) the surface-initiated polymerization of PMETAC brushes. Arrow indicates the shift in the critical angle.

surface-initiated polymerization. Taking into account that only 16% of amino groups are available for reacting and assuming that all of them reacted in the initiation step of the polymerization, it is possible to estimate the degree of polymerization (n) of the polymer brush. This has been done by normalizing to the equivalent intensity of surface amino groups that should have reacted ($0.16I_{SA}$), as expressed in eq 1:

$$n = \frac{I_{PMETAC} - I_{SA}}{0.16\, I_{SA}} \quad (1)$$

The obtained polymerization degree was $n = 32$, which implies that the polymer brush grew to the extent of becoming comparable to the pore diameter (~9 nm).

So far, XPS provided a detailed chemical analysis of the surface modification in the outer layers of the mesoporous film. To ensure that the brush growth proceeded homogeneously across the whole mesoporous film, i.e., inside the pores, we performed X-ray reflectivity (XRR) measurements on the chemically modified mesoporous samples. As was demonstrated by several authors,[29,30] XRR is a powerful technique to estimate density, porosity, and pore filling of mesoporous thin films from the analysis of the total reflection critical angles.

XRR measurements were performed under dry nitrogen flow that ensured 0% humidity conditions in order to avoid errors in the determination of film density due to water adsorption and/or condensation on the pore surface. XRR diagrams shown in Figure 2 reflect the changes in film electronic density due to the polymerization process occurring in the film. Two noticeable changes between the reflectivity data of the thin film prior to (amino-silica) and after polymerization (PMETAC-silica) are observed: an increase in the critical angle θ_c from 0.1800° to 0.1955° and the smoothing of the Kiessig fringes at higher angles. After the polymerization reaction, an increase in θ_c is observed, which correlates with an increase in density. The smoothing in the Kiessig fringes can be ascribed to a loss of contrast between the porous oxide matrix (now full of polymer) and the glass substrate. Both changes demonstrate the presence of polymer brush inside the pores and not only on the surface of the film. If the brush had preferably grown on the surface instead of inside the pores, i.e., forming a new polymer layer on top of the mesoporous film, we should have observed a second critical angle at lower θ_c values due to the less dense polymer layer, rather than a shift in the film critical angle. The presence of a unique θ_c shifted to higher angle, and the absence of significant changes in the overall thickness of the mesoporous film implies an increase in the density of the thin layer due to the grafting of the polymer inside the pore network, ruling out the formation of a polymer overlayer.

A quantitative analysis was carried out from XRR data in order to estimate the pore filling with the polymer brush. It is known that the electronic density ρ of a mesoporous films can be calculated directly from the measured θ_c[31]

$$\rho_{el} = \frac{\pi}{\lambda^2 r_e}\theta_c^2 \quad (2)$$

where λ is the X-ray wavelength and $r_e = 2.813 \times 10^{-6}$ nm is the classical radius of the electron. From the calculation of the electronic densities for both a mesoporous and a nonporous film, the volume fraction of mesopores, F_{pore}, can be estimated as

$$F_{pore} = 1 - \frac{\rho_{meso}}{\rho_{framework}} \quad (3)$$

where ρ_{meso} is the electronic density of the amino-modified mesoporous film and $\rho_{framework}$ is the electronic density of a nonmesoporous film with the same composition, produced under the same synthesis conditions and treatment, but in the absence of a mesoporous template.[29] Considering that the increase in film density is only due to the presence of PMETAC brushes, the volume fraction of polymer within the film, F_{PMETAC}, can be determined from the measured electronic densities according to

$$F_{PMETAC} = \frac{\rho_{meso+PMETAC} - \rho_{meso}}{\rho_{PMETAC}} \quad (4)$$

where $\rho_{meso+METAC}$ is the electronic density of film after polymerization, ρ_{meso} is the electronic density before polymerization (empty pores), and ρ_{PMETAC} is the brush electronic density calculated from planar substrates.[32] The mesopore filling fraction was 83%, as calculated from the ratio between the brush volume fraction F_{PMETAC} and the pore volume fraction F_{pore}. The most important implication of these results is that a large fraction of the pore volume is occupied by the polymer brush. These observations are in full agreement with the conclusions derived from XPS analysis indicating that the polymer chains grew to an extent comparable to the pore diameter (Figure 3).

Preconcentration Effect in PMETAC-Modified Mesoporous Silica Films: An Electrochemical Approach. Cyclic voltammetry (CV) was used to analyze the change in the transport properties of electrochemical probes. As recently demonstrated, changes in the voltammetric response of mesoporous electrodes reflect the changes in probe concentration or diffusion due to the architecture or electrostatic environment of the pores. It has been found that well-ordered mesostructures display enhanced transport properties of guest molecules compared to nonmesostructured architectures.[33] In addition, mesoporous films are able to preconcentrate solutes in the inner environment of the 3D pore array. Recently, Walcarius et al. demonstrated that the modification of ITO electrodes with mesoporous films can lead to a 1 order of magnitude enhancement of the voltammetric signal when

(29) Fuertes, M. C.; Marchena, M.; Marchi, M. C.; Wolosiuk, A.; Soler-Illia, G. J. A. A. *Small* **2009**, *5*, 272.
(30) Gibaud, A.; Hazra, S. *Curr. Sci.* **2000**, *78*, 1467.
(31) van der Lee, A. *Solid State Sci.* **2000**, *2*, 257.
(32) Azzaroni, O.; Brown, A. A.; Cheng, N.; Wei, A.; Jonas, A. M.; Huck, W. T. S. *J. Mater. Chem.* **2007**, *17*, 3433.
(33) (a) Walcarius, A.; Kuhn, A. *Trends Anal. Chem.* **2008**, *27*, 593. (b) Fattakhova-Rohlfing, D.; Wark, M.; Rathouský, J. *Chem. Mater.* **2007**, *19*, 1640.

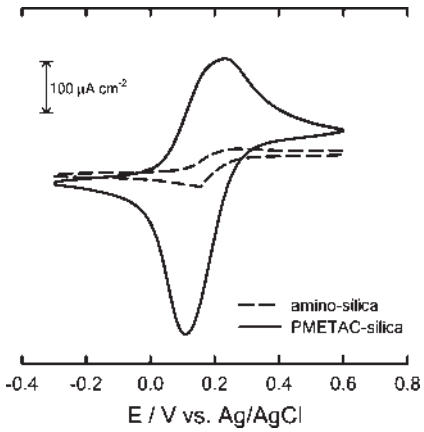

Figure 3. Cyclic voltammograms corresponding to ITO-supported amino-modified (dotted trace) and PMETAC brush-modified mesoporous silica films (solid trace) in the presence of redox probes in solution. Electrolyte: 1 mM $Fe(CN)_6^{3-}$ + 5 mM KCl. Scan rate: 100 mV s^{-1}.

Scheme 1. Schematical Description of the Confined Growth of the Polymer Brush within the Mesoporous Matrix: (a) Mesoporous Amino-Silica; (b) Brush-Modified Film after the Surface-Initiated Polymerization Reaction

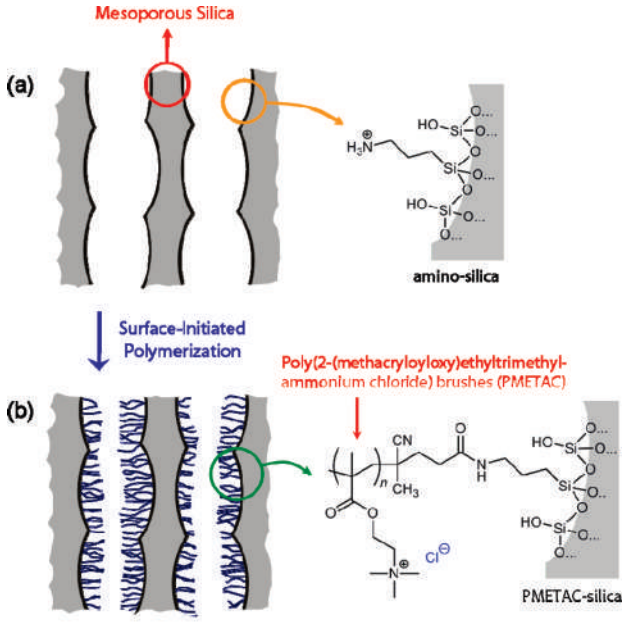

compared to the typical readouts measured on bare ITO surfaces.[34] In a similar vein, the modification of the mesoporous silica films with PMETAC brushes further enhanced the voltammetric signal of the redox probes dissolved in the electrolyte solution. Figure 3 shows the voltammograms corresponding to amino-functionalized (starting material) and PMETAC-brush modified silica films measured under the same experimental conditions, 100 mV s^{-1}.

Clearly, the presence of the PMETAC brush in the inner environment of the mesoporous network led to a dramatic preconcentration of the anionic probe within the hybrid film. The CV peak currents for $Fe(CN)_6^{3-}$ recorded with the PMETAC-modified films (205 μA cm^{-2}) were nearly 10 times higher that on amino-modified films (22 μA cm^{-2}).

Noteworthily, in spite of the high pore filling with the PMETAC brushes (83%), this polymer does not preclude the transport of anionic probes through the ordered mesoporous network. The strong electrostatic interaction between the $Fe(CN)_6^{3-}$ ions and the quaternary ammonium groups in the brush acts as a driving force to enhance the preconcentration of the redox probe in the mesoporous matrix. Considering that the voltammetric peaks (j_p) are proportional to $D^{1/2}C$ (being D the diffusion coefficient and C the concentration of the probe), we can infer that the local concentration of $Fe(CN)_6^{3-}$ in the brush-modified mesoporous matrix is significantly higher than that in solution. Recent experimental work has demonstrated that diffusion of $Fe(CN)_6^{3-}$ species through PMETAC brushes is much slower than that observed in electrolyte solutions;[35] hence, the probe concentration in the film must be notoriously higher than that in solution in order to fulfill the condition $j_p \propto D^{1/2}C$.

This preconcentration effect of the mesoporous film explains the experimental results described in the previous section, in which X-ray reflectivity demonstrated that PMETAC brush growth occurs almost exclusively within the mesoporous films. Hence, it is worth to remark at this point that the strong confinement/preconcentration effects may sensitively affect the kinetic characteristics of the polymerization reaction taking place in the pore environment. As a result, the polymerization rates of macromolecules grafted in the inner environment of the mesoporous films will differ from similar surface-initiated polymerizations occurring on a planar substrate.

Polymer growth proceeds in the presence of initiator-modified films constituted of amino-functionalized mesoporous silica substrates derivatized with 4,4′-azobis(4-cyanopentanoic acid). At neutral pH, i.e., polymerization conditions, the silanolate surface groups determine surface charge, generating an optimum environment to preconcentrate the cationic monomeric building blocks.[23] As the polymerization rate is proportional to the monomer concentration,[36] it is plausible to conclude that the polymer growth proceeds more rapidly inside the pore than on the outer surface.

Synthesis of Gold Nanoparticles inside Mesoporous Silica Films Modified with PMETAC Brushes. In the previous section we have shown and discussed the remarkable preconcentration properties of mesoporous hybrid thin films that permit to modify the pore surface with cationic polymer brushes. Taking advantage of the facile manipulation of the ionic environment of polyelectrolyte brushes by simple ionic exchange of their counterions, we proceeded to study the synthesis of Au nanoparticles via the chemical reduction of confined anionic $AuCl_4^-$ precursors. The nanoparticle synthesis involved a two-step process. First, Cl^- counterions in the as-synthesized PMETAC brushes were replaced by $AuCl_4^-$ species (pH ~ 1) via an ion exchange process. Subsequently, the gold chlorocomplexes were reduced with $NaBH_4$ to form the Au nanoparticles in the inner environment of the mesoporous film (Scheme 2).

In order to elucidate the role of the PMETAC brush in the confined synthesis of the Au nanoparticles, we performed similar experiments on the amino-functionalized mesoporous films that were used as precursors to the polymer-modified materials. These films contain a small fraction of NH_2 groups in pore walls that are protonated under acidic conditions. For the sake of comparison, we evaluated the extent of the Au NP synthesis within the pores by XRR characterization of both amino- and PMETAC

(34) Etienne, M.; Quach, A.; Grosso, D.; Nicole, L.; Sanchez, C.; Walcarius, A. *Chem. Mater.* **2007**, *19*, 844.

(35) Rodríguez Presa, M. J.; Gassa, L. M.; Azzaroni, O.; Gervasi, C. A. *Anal. Chem.* **2009**, *81*, 7936.

(36) Odian, G. In *Principles of Polymerization*; John Wiley & Sons: Hoboken, NJ, 2004.

Scheme 2. Schematic Depiction Describing the Synthesis of Metal Nanoparticles in the Inner Environment of the Mesoporous Film[a]

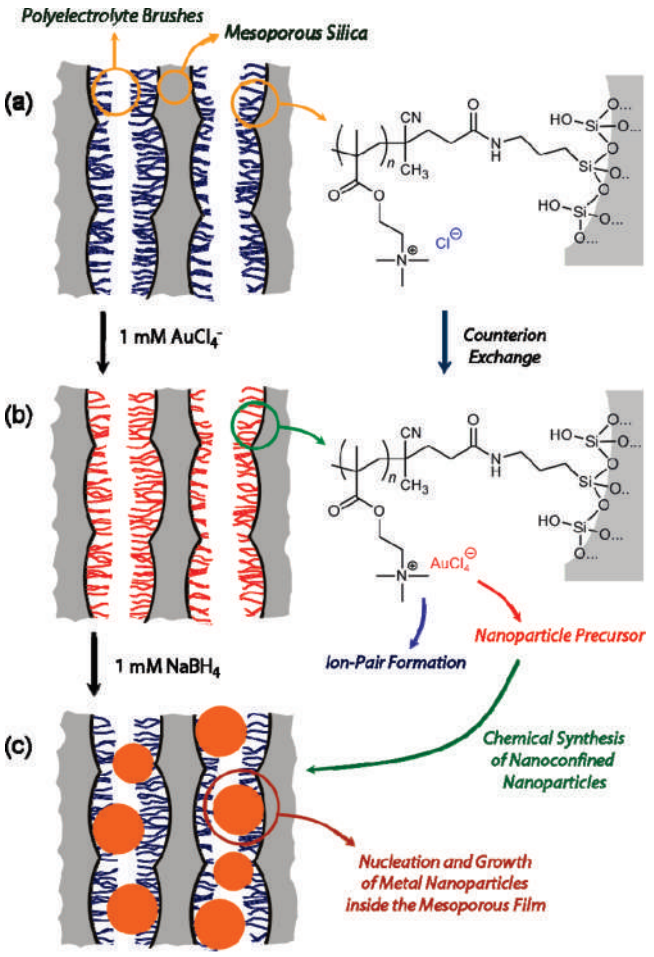

[a] The chloride counterions in the as-synthesized PMETAC-modified silica films (a) are exchanged by the corresponding anionic precursors, $AuCl_4^-$ (b). Then, the gold chlorocomplexes are chemically reduced to form metal nanoparticles within the nanoscale brush-coated pores (c).

brush-modified mesoporous samples, prior to and after growing the NPs (under the same experimental conditions).

As described above, a meaningful change in the electronic density of the films implies a shift in the critical angle θ_c; the reflectograms are very sensitive to the presence of metal nanoparticles in the mesopores.[29] Figure 4a shows that there are no appreciable changes in θ_c for amino-funcionalized films after a loading−reduction cycle of the $AuCl_4^-$ precursor. Conversely, PMETAC-modified samples evidence a well-defined shift in θ_c as well as an increase in the intensity of the Kiessig fringes. This implies that the electronic density of the brush-modified film increases after metal NP growth. The θ_c values are rather close to those determined in PMETAC-modified samples and significantly lower than those corresponding to a gold film ($\theta_c \sim 0.574°$). Hence, we can rule out the presence of a continuous thin metal film on top of the mesoporous substrate. This experimental evidence indicates that the Au NPs grew exclusively in the inner environment of the mesoporous network and solely in the samples modified with PMETAC brushes. In principle, we can hypothesize that amino-functionalized films are not able to preconcentrate enough gold precursors to nucleate metal nanoparticles inside the pores. This could be ascribed to the reduced number of positively charged groups responsible for anchoring the anionic precursors, compared to the $Si-O^-$ surface groups. In these amino-modified mesoporous

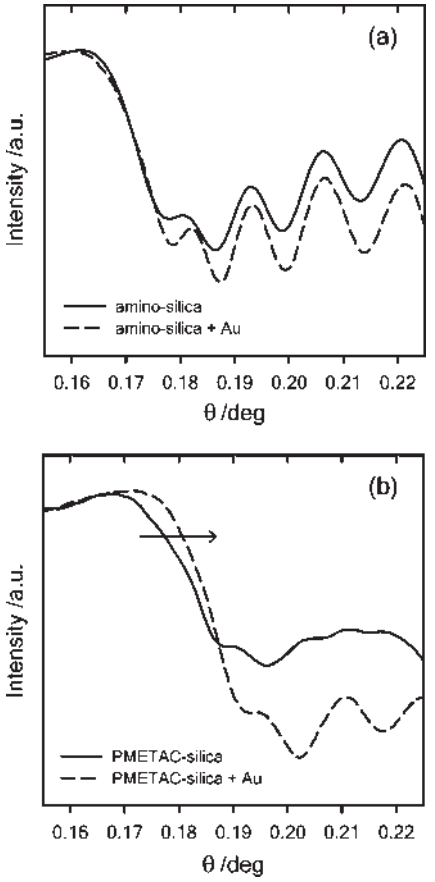

Figure 4. X-ray reflectograms corresponding to (a) amino-functionalized and (b) PMETAC-modified mesoporous silica films prior to (solid line) and after (dotted line) proceeding with the nanoparticle synthesis in the mesoporous scaffold. The arrow indicates the shift in the critical angle.

silica films, it has been observed that the surface charge is dominated by the acid−base behavior of the ≡Si−OH surface groups, which are more abundant than the protonated amino functions.[23]

From the analysis of the critical angle shifts, we obtained the filling factor for the Au NPs.[25] Our experimental results indicated that ~3% of the brush volume was occupied by Au NPs. This value is in close agreement with that reported for Au NPs synthesized in planar brushes under similar conditions, 7%.[32]

To visualize the nanomaterials synthesized inside the mesoporus film, we proceeded to the characterization of the samples prior to and after the synthesis of the Au colloids inside the pores by transmission electron microscopy (TEM) (Figure 5a,b). Figure 5c shows the characteristic 2D-SAXS pattern of a mesoporous sample thermally treated at 200 °C corresponding to a pore array derived from the uniaxial contraction of an $Im\bar{3}m$ cubic mesostructure. The spot pattern corroborates the long-range pore order and orientation in these hybrid systems. This pore framework provides an organized array of interconnected nanoreactors of ellipsoidal shape (see above) for carrying out the colloidal synthesis in the confined environment. Figure 5b shows a TEM micrograph of the mesostructured films after synthesizing the Au nanoparticles (darker regions) inside the mesopores. Under the TEM observation conditions employed (65 kV), it is typically very difficult to focus the mesoporous oxide−polymer matrix and the metal NP simultaneously due to the differences in their electronic densities. For the sake of clarity, only Au-NPs were properly focused in order to visualize the confined colloids and estimate their size. The histogram of NP diameters (d) obtained by

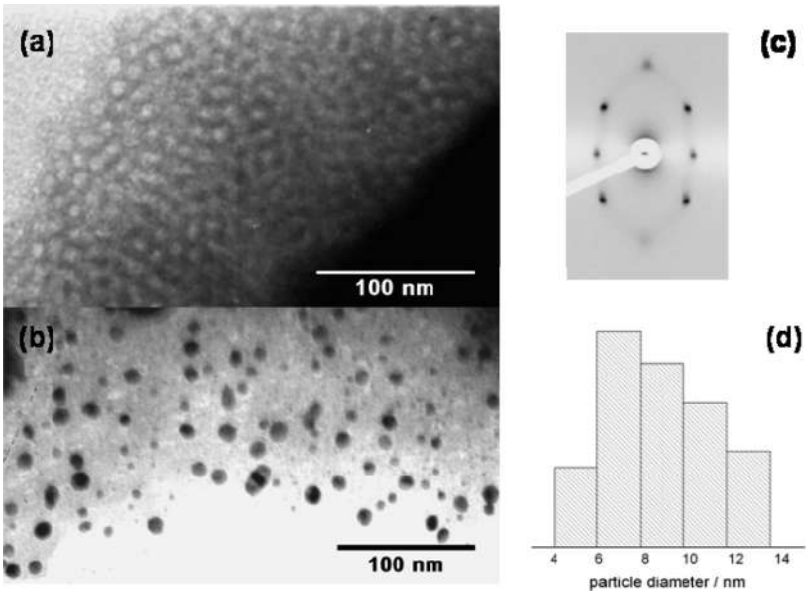

Figure 5. TEM images of PMETAC-modified mesoporous silicon samples prior to (a) and after (b) synthesizing the confined Au NPs. (c) SAXS-2D pattern of amino-functionalized mesoporous films. (d) Histogram of Au-NP diameters, $\langle d \rangle$, obtained from TEM image analysis.

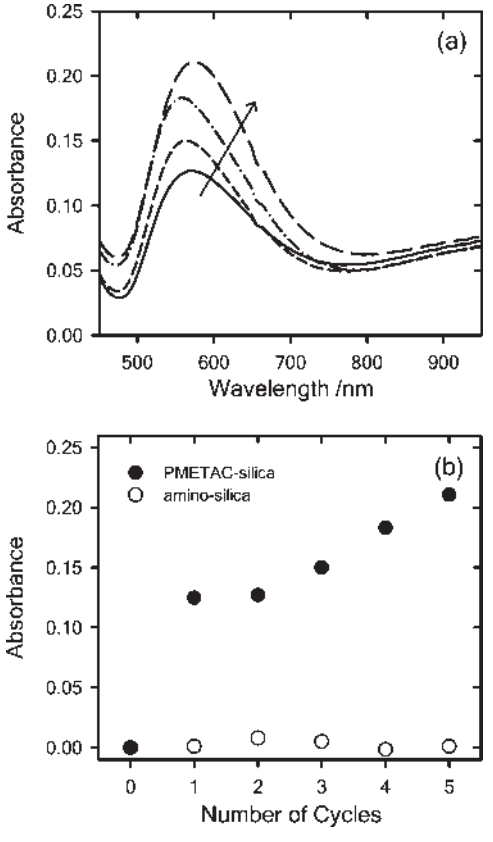

Figure 6. (a) UV−vis spectrum of Au-NP-loaded PMETAC-modified samples after consecutive "loading" cycles. (b) Evolution of plasmon resonance intensity of Au NPs confined in PMETAC-modified (●) and amino-modified (○) mesoporous films upon increasing "loading" cycles.

analysis of the top-view TEM images (Figure 6d) shows an asymmetric distribution with $\langle d \rangle$ corresponding to 8 nm. It is worthwhile indicating that the contributions from larger diameters (10−14 nm) could be attributed to the presence of some interconnected NPs or to the overlapping of particles in transmission conditions. Notwithstanding this observation, the average Au-NP diameter is in good agreement with the pore dimensions of the Pluronics F127 templated films along the *xy* plane (i.e., the major axis of the ellipsoidal mesopores) obtained by ellipsometric porosimetry (see Supporting Information). As also shown in a previous work, the mesoporous matrix is controlling the NP maximum size but not their distribution. The gold NPs are not forming an ordered array, but they are homogeneously distributed inside the porous network in the reported reduction conditions.[29]

To evaluate the optical properties of Au-NP inside PMETAC-modified films, we tracked the evolution of their plasmon absorption by UV−vis spectroscopy performed on mesoporous films deposited on transparent substrates (Figure 6).

Typical UV−vis spectra of Au NPs synthesized within silica mesoporous films show a strong and broad absorption band with a maximum in the 500−600 nm region due to Au plasmonic oscillations. Figure 6a shows the evolution of Au-NP plasmonic oscillations after consecutive NP loading−reduction cycles (i.e., $AuCl_4^-$ preconcentration in the PMETAC-modified film followed by the chemical reduction with $NaBH_4$). To illustrate the key role of the PMETAC brushes in the loading of the metal NPs, we also plotted the absorbance values obtained from similar experiments performed in the amino-functionalized (i.e., "PMETAC brush-free") mesoporous silica films. The mesoporous films with PMETAC brushes display intense plasmonic signals whereas films without METAC did not evidence any significant absorption under the same experimental conditions. This is a strong indication that PMETAC films act as macromolecular building blocks assisting and enhancing the production of metal nanoparticles inside the mesoporous film.

The light absorption properties of the films are due to the nanoparticle size and shape as well as the refractive index of the matrix in which the NP are embedded. In previous work it has been observed that the reduction process within mesopores to obtain metallic nanoparticles can lead either to isolated particles that copy the pore shape (in mild reducing conditions) or to interconnected arrays (for stronger reducing agents or prolonged

reduction treatment) when these nanoparticles grow and develop interconnection.[37] Plasmon band position is related to particle size and shape.[38] Rod-shaped gold nanoparticles, for example, absorb at 700−800 nm. For low Au loadings, the plasmon band maximum is located at 570 nm. This position is compatible with isolated nanoparticles of spherical or ellipsoidal shape included in an oxide matrix. For higher Au loadings (i.e., several adsorption−reduction cycles), we observe a slight bathochromic shift of the plasmon bands, accompanied by the emergence of a low absorption shoulder at ca. 700 nm. This effect can be ascribed to some NP interconnection that can develop upon higher NP loading after repeated reduction cycles. Interconnected NP can present light absorption in the 650−700 nm region, similarly to elongated objects.[29] In summary, we observe that the modified mesopore system helps to preconcentrate the negatively charged Au(III) precursor. Discrete Au nanoparticles can be included within the films following a mild reduction treatment. Repeated reduction cycles can lead to the presence of a small fraction of interconnected NP that behave as elongated objects, presenting absorption at longer wavelengths.

Conclusions

We have demonstrated a facile and robust methodology allowing the controlled confinement of metal nanoparticles within the 3D framework of mesoporous silica thin films. The chemical strategy is based on a surface-modification scheme using polyelectrolyte brushes as building blocks to enhance the preconcentration of nanoparticle precursors in the inner environment of the mesoporous film. We have shown that the functionalization of the mesoporous framework with cationic polyelectrolyte brushes is the key factor allowing the formation of metal colloids locally addressed into the mesopores. Preconcentration effects driven by the controlled surface charge are responsible for the site-selective character of the different chemistries taking place in the film in each step. The method can be extended in principle to the functionalization of the pore walls with different polymer brushes in order to tune the monomer−precursor interactions and assist the preconcentration of selected guest molecules in the pore system.

As a general idea, we demonstrate that we can take advantage of the synergy taking place between two versatile functional nanobuilding blocks such as ordered mesopores and polymer brushes in order to produce a stable nanocomposite with tuned optical properties. The ability to control the 3D mesostructure is a key advantage for creating functional platforms through the rational design of *chemistry* and *topology* in confined environments. This concept can be in principle extended to complex multilayer or patterned systems, in order to achieve systems with well-defined physical and chemical properties in arbitrary locations.[38] Polymer brush-functionalized mesoporous hybrid thin films represent a valuable example of the integration of inorganic, polymer, and physical chemistry, a core concept to design, create, and manipulate complex hierarchical nanoarchitectures.[39−41]

Acknowledgment. The authors ackowledge financial support from Agencia Nacional de Promoción Científica y Tecnológica (PICT 34518, PAE 2004 22711), Centro Interdisciplinario de Nanociencia y Nanotecnología (CINN, PAE 2006 37063, projects: PRH 2007-74-PIDRI No. 74, and PME 00038), Gabbos (DG-017), Max-Planck-Gesellschaft (MPG), Alexander von Humbolt Stiftung, Laboratório Nacional de Luz Síncrotron (LNLS), Higher Education Commission (HEC) of Pakistan and Deutscher Akademischer Austauschdienst (DAAD) (Code #A/04/30795). The authors are grateful to Laura Saldarriaga for helpful assistance in the ellipsometric porosimetry measurements. A.C. acknowledges CONICET and TENARIS for a scholarship. M.C.F. acknowledges CONICET for a doctoral fellowship. F.J.W., O.A. and G.J.A.A.S.-I. are CONICET fellows.

Supporting Information Available: Figure showing water adsorption−desorption isotherm of a 20% amino-containing mesoporous silica thin film and its pore size distribution. This material is available free of charge via the Internet at http://pubs.acs.org.

(37) Pérez, M. D.; Otal, E.; Bilmes, S. A.; Soler-Illia, G. J. A. A.; Crepaldi, E. L.; Grosso, D.; Sanchez, C. *Langmuir* **2004**, *20*, 29.

(38) (a) Myroshnychenko, V.; Rodríguez-Fernández, J.; Pastoriza-Santos, I.; Funston, A. M.; Novo, C.; Mulvaney, P.; Liz-Marzán, L. M.; García de Abajo, F. J. *Chem. Soc. Rev.* **2008**, *37*, 1792. (b) Eustis, S.; El-Sayed, M. *Chem. Soc. Rev.* **2006**, *35*, 209.

(39) (a) Angelomé, P. C.; Fuertes, M. C.; Soler-Illia, G. J. A. A. *Adv. Mater.* **2006**, *18*, 2397. (b) Fuertes, M. C.; López-Alcaraz, F. J.; Marchi, M. C.; Troiani, H.; Luca, V.; Míguez, H.; Soler-Illia, G. J. A. A. *Adv. Funct. Mater.* **2007**, *17*, 1247. (c) Martínez, E. D.; Bellino, M. G.; Soler-Illia, G. J. A. A. *ACS Appl. Mater. Interface* **2009**, *1*, 746.

(40) (a) Prouzet, E.; Ravaine, S.; Sanchez, C.; Backov, R. *New J. Chem.* **2008**, *32*, 1284. (b) Dujardin, E.; Mann, S. *Adv. Mater.* **2002**, *14*, 775–788. (c) Fowler, C. E.; Khushalani, D.; Lebeau, B.; Mann., S. *Adv. Mater.* **2001**, *13*, 649–652. (d) Bein, T. In*Supramolecular Architecture: Synthetic Control in Thin Films and Solids*; Bein, T., Ed.; American Chemical Society: Washington, DC, 1992; Chapter 1, pp 1−7.

(41) Sanchez, C.; Giraud Guille, M. M.; Arribart., H. *Nat. Mater.* **2005**, *4*, 277.